44 Assadi M, Janson C, Wang DJ *et al.* Lithium citrate reduces excessive intra-cerebral N-acetyl aspartate in Canavan disease. *Eur. J. Paediatr. Neurol.* 2010; **14**: 354–9.
45 Arun P, Madhavarao CN, Moffett JR *et al.* Metabolic acetate therapy improves phenotype in the tremor rat model of Canavan disease. *J. Inherit. Metab. Dis.* 2010; **33**: 195–210.
46 Mathew R, Arun P, Madhavarao CN, Moffett JR, Namboodiri MA. Progress toward acetate supplementation therapy for Canavan disease: Glyceryl triacetate administration increases acetate, but not N-acetylaspartate, levels in brain. *J. Pharmacol. Exp. Ther.* 2005; **315**: 297–303.
47 Segel R, Anikster Y, Zevin S *et al.* A safety trial of high dose glyceryl triacetate for Canavan disease. *Mol. Genet. Metab.* 2011; **103**: 203–6.
48 Roe CR, Mochel F. Anaplerotic diet therapy in inherited metabolic disease: Therapeutic potential. *J. Inherit. Metab. Dis.* 2006; **29**: 332–40.
49 Marin-Valencia I, Roe CR, Pascual JM. Pyruvate carboxylase deficiency: Mechanisms, mimics and anaplerosis. *Mol. Genet. Metab.* 2010; **101**: 9–17.
50 Francis JS, Markov V, Leone P. Dietary triheptanoin rescues oligodendrocyte loss, dysmyelination and motor function in the nur7 mouse model of Canavan disease. *J. Inherit. Metab. Dis.* 2014; **37**: 369–81.
51 Pederzolli CD, Rockenbach FJ, Zanin FR *et al.* Intracerebroventricular administration of N-acetylaspartic acid impairs antioxidant defenses and promotes protein oxidation in cerebral cortex of rats. *Metab. Brain Dis.* 2009; **24**: 283–98.
52 Leone P, Shera D, McPhee SW *et al.* Long-term follow-up after gene therapy for Canavan disease. *Sci. Transl. Med.* 2012; **4**: 165ra63.
53 Ahmed SS, Gao G. Gene therapy for Canavan's disease takes a step forward. *Mol. Ther.* 2013; **21**: 505–6.

LETTER

doi:10.1038/nature12500

Two replication fork maintenance pathways fuse inverted repeats to rearrange chromosomes

Lingchuan Hu[1]*, Tae Moon Kim[1]*, Mi Young Son[1], Sung-A Kim[1], Cory L. Holland[1], Satoshi Tateishi[2], Dong Hyun Kim[1], P. Renee Yew[1], Cristina Montagna[3], Lavinia C. Dumitrache[1]† & Paul Hasty[1]

Replication fork maintenance pathways preserve chromosomes, but their faulty application at nonallelic repeats could generate rearrangements causing cancer, genomic disorders and speciation[1–3]. Potential causal mechanisms are homologous recombination and error-free postreplication repair (EF-PRR). Homologous recombination repairs damage-induced DNA double-strand breaks (DSBs) and single-ended DSBs within replication. To facilitate homologous recombination, the recombinase RAD51 and mediator BRCA2 form a filament on the 3′ DNA strand at a break to enable annealing to the complementary sister chromatid[4] while the RecQ helicase, BLM (Bloom syndrome mutated) suppresses crossing over to prevent recombination[5]. Homologous recombination also stabilizes[6,7] and restarts[8,9] replication forks without a DSB[10,11]. EF-PRR bypasses DNA incongruities that impede replication by ubiquitinating PCNA (proliferating cell nuclear antigen) using the RAD6–RAD18 and UBC13–MMS2–RAD5 ubiquitin ligase complexes[12]. Some components are common to both homologous recombination and EF-PRR such as RAD51 and RAD18[13,14]. Here we delineate two pathways that spontaneously fuse inverted repeats to generate unstable chromosomal rearrangements in wild-type mouse embryonic stem (ES) cells. Gamma-radiation induced a BLM-regulated pathway that selectively fused identical, but not mismatched, repeats. By contrast, ultraviolet light induced a RAD18-dependent pathway that efficiently fused mismatched repeats. Furthermore, TREX2 (a 3′→5′ exonuclease) suppressed identical repeat fusion but enhanced mismatched repeat fusion, clearly separating these pathways. TREX2 associated with UBC13 and enhanced PCNA ubiquitination in response to ultraviolet light, consistent with it being a novel member of EF-PRR. RAD18 and TREX2 also suppressed replication fork stalling in response to nucleotide depletion. Interestingly, replication fork stalling induced fusion for identical and mismatched repeats, implicating faulty replication as a causal mechanism for both pathways.

The identical and mismatched repeat reporters (IRR and MRR, Fig. 1a, b) were designed to investigate pathways that rearrange chromosomes through repeat fusion. Both reporters contain a 313-base-pair major satellite repeat (MSR) at each junction of an inversion in *miniHPRT*. These repeats are indirect so repeat fusion restores *miniHPRT* to enable survival in hypoxanthine, aminopterin, thymidine (HAT)-selection media by a potential mechanism shown in Fig. 1c. The only difference between these reporters is that the MRR 3′ repeat contains seven mismatches with the longest contiguous homology being 67 bases. The IRR and MRR were stably transfected into wild-type AB2.2 and IB10 ES cells. About the same number of HAT-resistant colonies spontaneously grew for both reporters (Fig. 1d, $P > 0.85$, Student's *t*-test), indicating that spontaneous repeat fusion occurred in wild-type cells.

The fused 5′ repeat for the MRR was sequenced to determine the switch location (Fig. 1e, Extended Data Fig. 1). Strand exchange in fission yeast predominantly occurred at the palindrome centre after replication forks were induced to stall, an event called a U turn[9]. We found 6 of 14 switches had this U-turn at the base of a putative hairpin (all green), whereas two occurred at the apex (all orange) and six occurred in the stem (green-orange). Thus, strand exchange occurred at multiple locations.

It is possible that the switched strand replicated to the telomere, forming a dipericentric (Fig. 1c). Two-colour fluorescence *in situ* hybridization (FISH) was performed on clones with the IRR and MRR using a pericentromeric and telomeric probe. Dipericentrics and chromosomes with extra pericentromeres and telomeres (EPTs)[15] were observed for cells with both reporters (Extended Data Fig. 2a and Extended Data Tables 1 and 2). EPTs seemed unstable because the pericentromere number and location varied between metaphase spreads from the same clone, implicating secondary events consistent with breakage–fusion–bridge cycles[16]. Spectral karyotyping on three MRR clones showed multiple fusion points confirming rearrangement complexity (Extended Data Table 3). Duplications of chromosome 1 (Fig. 1f, left) and translocations between chromosomes 14 and 11 (Fig. 1f, right) or 14 and 13 were frequently observed from the same clone and even in the same metaphase spread, indicating a role in genome topology[17]. Two-colour FISH was performed on a single clone (clone 18 from Extended Data Tables 2 and 3) with the MRR probe and either chromosome 1 or 14. This analysis revealed unstable structures because the MRR could be found at either chromosomes 1 or 14 (Extended Data Fig. 2b), indicating faulty DNA synthesis[18]. Furthermore, the MRR pattern changed from a discrete dot to multiple dots interspersed with chromosomal sequences similar to segmental duplications described during evolution[19]. Thus, both reporters caused unstable and complex rearrangements, yet the causal pathways are not known.

Complex genomic rearrangements could arise from faulty chromosome maintenance. Therefore, we tested whether γ-radiation or ultraviolet light enhanced repeat fusion for wild-type AB2.2 cells with the IRR or MRR. Exposure to 4 Gy γ-radiation induced repeat fusion for the IRR (Fig. 2a, left, $P = 0.017$, Student's *t*-test) but not the MRR (Fig. 2a, right, $P = 0.16$), whereas exposure to 20 J m^{-2} ultraviolet light had the opposite effect on the IRR (Fig. 2b, left, $P = 0.35$) and MRR (Fig. 2b right, $P = 0.006$). This contrast suggests different pathways fused identical and mismatched repeats.

We tested whether homologous recombination proteins fused identical repeats because homologous recombination corrects damage caused by γ-radiation but not ultraviolet light[4]. We tested BLM-defective ES cells ($blm^{tm3Brd/tm4Brd}$, simply called $blm^{-/-}$)[20] because BLM regulates homologous recombination through Holliday junction dissolution[5]. Repeat fusion was significantly higher in $blm^{-/-}$ cells as compared to AB2.2 cells for the IRR (Fig. 2c, compare lanes 1 and 2, $P < 0.0001$), but not the MRR (Fig. 2c, compare lanes 6 and 7, $P = 0.47$). Next we tested $blm^{-/-}$ cells haploinsufficient for RAD51 or BRCA2 because BRCA2 enables RAD51 filament formation on DNA single stands to mediate strand annealing and Holliday junction formation. We found $blm^{-/-}$ $Rad51^{+/\Delta ex2\text{-}4}$ cells

[1]Department of Molecular Medicine/Institute of Biotechnology, The Barshop Institute for Longevity and Aging Studies, The University of Texas Health Science Center at San Antonio, 15355 Lambda Drive, San Antonio, Texas 78245-3207, USA. [2]Institute of Molecular Embryology and Genetics (IMEG), Kumamoto University, Honjo 2-2-1 Kumamoto 860-0811, Japan. [3]Department of Genetics, Albert Einstein College of Medicine of Yeshiva University, Bronx, New York 10461, USA. †Present address: Department of Genetics & Tumor Cell Biology M/S 331, St Jude Children's Research Hospital, 262 Danny Thomas Place, Memphis, Tennessee 38105, USA.
*These authors contributed equally to this work.

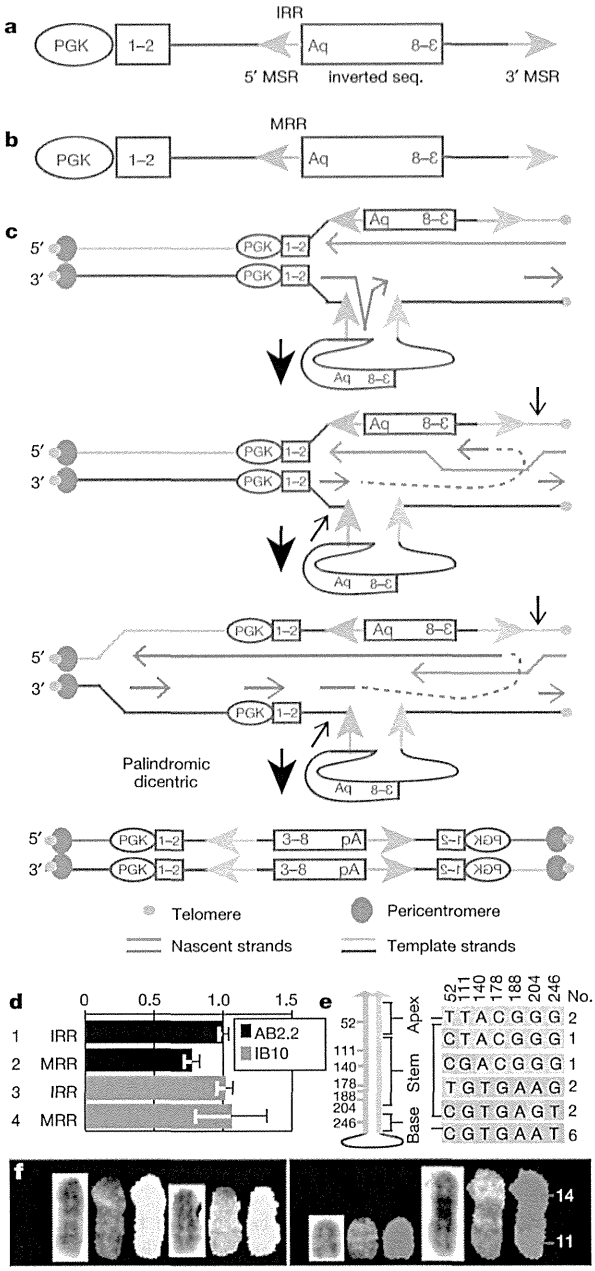

Figure 1 | Inverted repeat fusion. **a**, **b**, *MiniHPRT* reporters. Promoter (PGK) with intron that separates exons 1 and 2 from 3–8. Repeats at inversion junction. The IRR (**a**) and MRR (**b**) differ only in seven 3′ repeat mismatches (green vs orange arrow). **c**, Repeat fusion model. From top to bottom, nascent lagging strand stalls at repeat hairpin and switches to displace complementary template strand to correct *miniHPRT* and produce a dipericentric. **d**, Repeat fusion in AB2.2 and IB10 cells. Shown is the ratio of HAT-resistant colonies compared to IRR. Percentages of HAT-resistant colonies for the IRR in AB2.2 and IB10 are 0.02% and 0.14%, respectively. Biological replicates for lanes 1–4: 19, 19, 18 and 18, respectively. Error bars, standard error of the mean (s.e.m.). **e**, Sequence of fused repeats for the MRR in AB2.2 cells (Extended Data Fig. 1). **f**, Spectral karyotyping analysis on clone 18 (Extended Data Table 3). Left, duplication of chromosome 1; right, translocation of chromosomes 11 and 14.

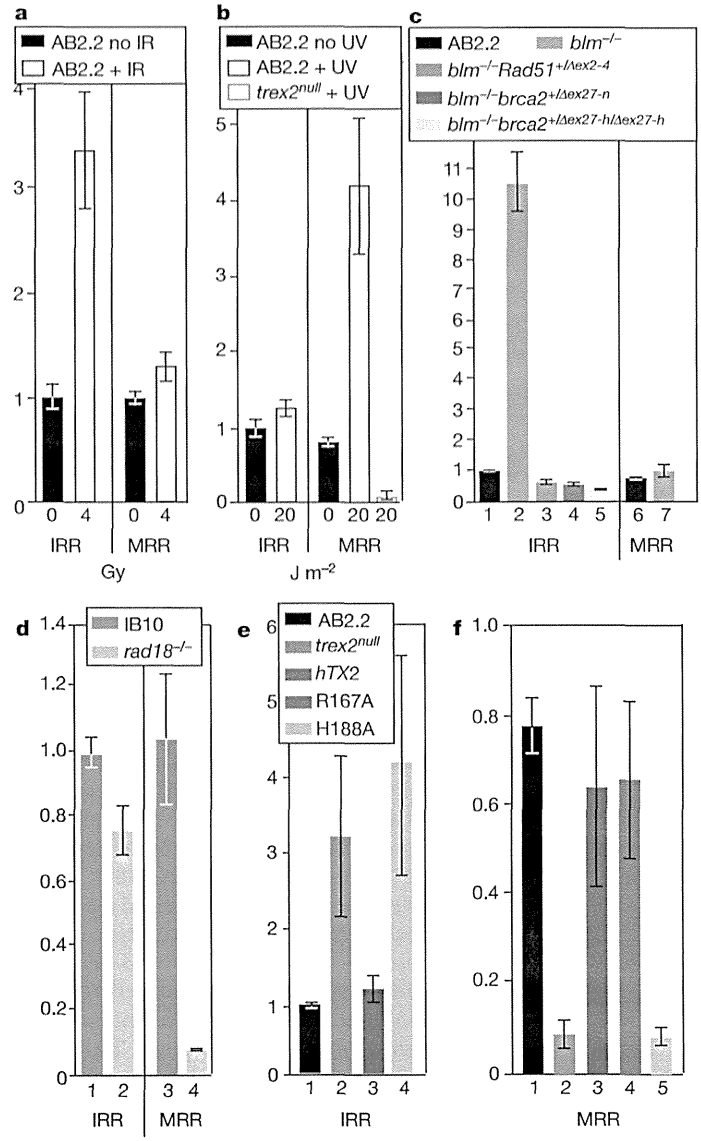

Figure 2 | Two pathways enable repeat fusion that depend on sequence identity. Shown is the ratio of HAT-resistant colonies transfected with IRR in control cells displayed in Fig. 1d. **a**, Gamma radiation (4 Gy) increases fusion for the IRR (left) but not MRR (right). Survival fraction, ~10%. Biological replicates for lanes 1–4: 19, 11, 19 and 11, respectively. **b**, Ultraviolet light (20 J m^{-2}) enables fusion for the MRR (right) but not IRR (left). Survival fraction, ~0.6%. Biological replicates for lanes 1–4: 19, 11, 19 and 11, respectively. **c**, BLM suppressed repeat fusion for the IRR but not MRR. $blm^{-/-}$ cells deleted for one copy of *Rad51* exons 2–4 ($blm^{-/-}$ $Rad51^{+/\Delta ex2\text{-}4}$ cells), one copy of *Brca2* exon 27 ($blm^{-/-}$ $brca2^{+/\Delta ex27\text{-}n}$) or two copies of *Brca2* exon 27 ($blm^{-/-}$ $brca2^{\Delta ex27\text{-}h/\Delta ex27\text{-}n}$). Biological replicates for lanes 1–7: 19, 23, 12, 12, 12, 19 and 23, respectively. **d**, RAD18 enabled fusion for the MRR more than IRR. Biological replicates: 18 for all lanes. **e**, **f**, TREX2 suppressed fusion for the IRR (**e**) but enabled fusion for the MRR (**f**). Examined are $trex2^{null}$ cells that express human wild-type *TREX2* (*hTX2*) or human *TREX2* mutated in the DNA binding domain (R167A) or catalytic domain (H188A). Biological replicates for lanes 1–4 in **e**: 19, 19, 20, and 23, respectively, and for lanes 1–5 in **f**: 19, 21, 21, 21 and 23, respectively. Error bars show s.e.m. throughout.

(Extended Data Fig. 3) and $blm^{-/-}$ $brca2^{+/\Delta ex27\text{-}n}$ cells (Extended Data Fig. 4a) showed reduced repeat fusion (Fig. 2c, compare lane 2 to 3 and 4, $P < 0.0001$). Deleting the remaining *Brca2* exon 27 copy (Extended Data Fig. 4b) further reduced repeat fusion (Fig. 2c, compare lanes 4 and 5, $P = 0.049$). Thus, BLM suppressed RAD51/BRCA2-mediated identical repeat fusion consistent with an homologous-recombination-based pathway (these data do not address the potential role of RAD51/BRCA2 in mismatch repeat fusion).

We tested if EF-PRR fused mismatched repeats because ultraviolet light, but not γ-radiation, induced PCNA ubiquitination in mammalian cells[21]. IB10 ES cells deleted for RAD18 (ref. 22) were analysed. These cells showed slightly lower levels of repeat fusion for the IRR as compared to IB10 control cells (Fig. 2d, compare lanes 1 and 2, $P = 0.06$). This reduction could reflect the nonessential participation of RAD18 in homologous recombination[14]. By contrast, RAD18-deletion significantly

lowered fusion of mismatched repeats (Fig. 2d, compare lanes 3 and 4, $P = 0.0005$). The reduction of mismatched repeat fusion is greater than identical repeat fusion ($P < 0.0001$), demonstrating that the role of RAD18 in fusing mismatched repeats is more prominent than identical repeats. These results are consistent with EF-PRR fusing mismatched repeats. Yet, RAD18 is an E3 ubiquitin ligase so it could have broad function; therefore, mutations in other genes in the poorly understood EF-PRR pathway should be observed.

TREX2 could be a novel member of EF-PRR. Previously, we analysed *trex2*^{null} cells and cells that expressed wild-type human *TREX2* (TREX2^{WT}) and human TREX2 mutated in the catalytic domain (TREX2(H188A)) and DNA-binding domain (TREX2(R167A), ~85% reduction in DNA binding)[23,24]. We found TREX2 deletion elevated levels of spontaneous isochromatid breaks and chromosomal rearrangements[24,25]. TREX2^{WT} rescued the null phenotype whereas TREX2(H188A) exacerbated this phenotype, suggesting a dominant effect[24]. These observations suggested defective DSB repair. However, *trex2*^{null} cells exhibited increased DSB repair and normal BLM-regulated sister chromatid exchanges (SCEs)[26]. Therefore, we proposed that TREX2 did not repair DSBs but instead suppressed DSB formation through an unknown pathway, possibly EF-PRR. In support, *trex2*^{null} cells had reduced levels of spontaneous SCEs[26,27].

TREX2-altered cells were tested for fusion of identical and mismatched repeats. *trex2*^{null} and TREX2(H188A)-expressing cells had elevated levels of identical repeat fusion as compared to control cells (AB2.2 and *Trex2*^{hTX2} cells) (Fig. 2e, compare lanes 1 and 3 to 2 and 4, $P < 0.05$), corroborating our previous observations that homologous recombination is elevated in *trex2*^{null} cells and that an homologous-recombination-based pathway fuses identical repeats. A similar anti-recombination effect on identical repeats was seen for the 3′ exonucleases ExoI and ExoVII in *Escherichia coli*, suggesting that 3′ exonuclease activity inhibits these fusions[28]. We also found *trex2*^{null} and TREX2(H188A)-expressing cells had very low levels of mismatch repeat fusion as compared to AB2.2, *Trex2*^{hTX2} and *Trex2(R167A)* cells (Fig. 2f, compare lanes 1, 3 and 4 to 2 and 5, $P < 0.0006$). Furthermore, TREX2-mediated ultraviolet-light-induced fusion of mismatched repeats (Fig. 2b right panel, $P = 0.003$). These data clearly separate the pathways that mediate identical and mismatch repeat fusion and demonstrate sequence identity determined pathway choice. These data also demonstrate the importance of the catalytic activity of TREX2 in mediating repeat fusion. Exonuclease activity would predictably remove intermediate 3′ mismatches or flaps that could occur at the DNA incongruity or during strand exchange and strand displacement. Furthermore, these data are consistent with TREX2 being part of the EF-PRR machinery.

Three experiments were performed to test if TREX2 is a member of EF-PRR. First, TREX2 located to the nascent replication strand after ultraviolet light exposure (Extended Data Fig. 5a); thus, it was at the right place at the right time. Second, TREX2 associated with UBC13, but not MMS2, by glutathione-*S*-transferase (GST) pull-down (Extended Data Fig. 5b); UBC13–MMS2 is the E2 heterodimer that polyubiquitinates PCNA[12,21]. In addition, TREX2 associated with UBC13 after ectopic expression in HeLa cells that was enhanced by ultraviolet light (Extended Data Fig. 5c); thus, it associated with the PCNA ubiquitination machinery. Third, we tested the impact TREX2 and RAD18 had on PCNA ubiquitination. As a control we found ultraviolet light, but not γ-radiation, enhanced PCNA ubiquitination as previously seen in human cells[21] (Extended Data Fig. 6a). TREX2 and RAD18 were needed for efficient PCNA ubiquitination after exposure to ultraviolet light (Extended Data Fig. 6b–d). In addition, cells deleted for both RAD18 and TREX2 (Extended Data Fig. 7) showed no further reduction in PCNA ubiquitination, indicating that they are epistatic (Extended Data Fig. 6b–d). These observations are consistent with TREX2 being part of the EF-PRR machinery and implicate RAD18 and TREX2 in replication fork maintenance.

Potential mechanisms for repeat fusion are faulty DNA repair and faulty DNA replication[2]. Repeat fusion could manifest from faulty

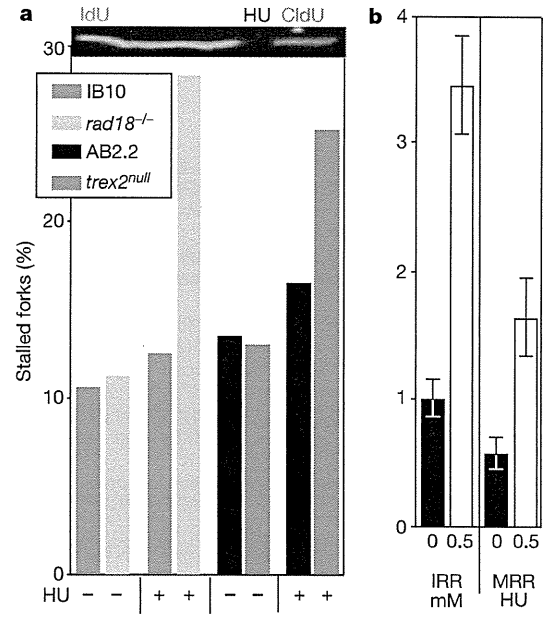

Figure 3 | Hydroxyurea-induced nucleotide depletion. a, RAD18 and TREX2 maintain replication forks. The percentage of stalled replication forks after hydroxyurea exposure is shown. Experimental design: cells were cultured in IdU (5-iodo-2′-deoxyuridine) (20 min) to label nascent strand and then exposed to hydroxyurea (0.5 mM, 90 min) to stall replication and then cultured in CldU (5-chloro-2′-deoxyuridine) (20 min) to label restart. Fibre number observed without and with hydroxyurea: IB10 (1,943, 657), *rad18*$^{-/-}$ (1,180, 1,460), AB2.2 (452, 510), *trex2*^{null} (705, 448). **b**, The impact of hydroxyurea (0.5 mM, 90 min) on repeat fusion for the IRR (left) and MRR (right). The ratio of HAT-resistant colonies as compared to AB2.2 cells transfected with the IRR (0.05%) is shown. Survival fraction is 100%. Error bars, s.e.m. Biological replicates, 6 for all lanes.

DNA repair since γ-radiation and ultraviolet light increased fusion. However, the odds that damage actually occurred in or near the reporter sequences is small (even after exposure to agent); thus, the agents could cause a compensatory increase in repair pathways. RAD51, BRCA2 and BLM are involved in both DSB repair and replication fork maintenance[6,7,10,11,15,29] so either are possible while direct evidence that RAD18 and TREX2 maintain replication forks is lacking in mammalian cells. Therefore, *rad18*$^{-/-}$ and *trex2*^{null} cells were exposed to a brief pulse of low concentration hydroxyurea (0.5 mM, 90 min) that depletes nucleotides to stall replication forks without causing DSBs[6,7,10,29]. We found *rad18*$^{-/-}$ and *trex2*^{null} cells had elevated levels of stalled replication forks compared to control cells (Fig. 3a, $P < 0.0001$) similar to depletion of the RAD5 orthologue, HLTF[30]. We further tested faulty replication as causal for repeat fusion by exposing cells with the IRR or MRR to this mild hydroxyurea concentration (Fig. 3b). This exposure increased repeat fusion for the IRR ($P = 0.00025$, Student's *t*-test) and MRR ($P = 0.0037$). Our observations suggest a BLM-regulated pathway consistent with homologous recombination fused identical repeats whereas a RAD18/TREX2-dependent pathway consistent with EF-PRR fused mismatched repeats during replicative stress. These pathways are good candidates for causing complex rearrangements found in cancer and genomic disorders in people and chromosomal variation that leads to species diversification.

METHODS SUMMARY

Repeat fusion assay: the reporters were randomly integrated into ES cells, selected in HAT and colonies counted (colonies were also counted without selection to control for seeding efficiencies). The percentage of HAT-resistant colonies was determined by dividing the number of HAT-resistant colonies by the number of cells electroporated multiplied by the seeding efficiency.

Online Content Any additional Methods, Extended Data display items and Source Data are available in the online version of the paper; references unique to these sections appear only in the online paper.

Received 2 January; accepted 22 July 2013.
Published online 8 September 2013.

1. Hastings, P. J., Lupski, J. R., Rosenberg, S. M. & Ira, G. Mechanisms of change in gene copy number. *Nature Rev. Genet.* **10,** 551–564 (2009).
2. Carr, A. M., Paek, A. L. & Weinert, T. DNA replication: failures and inverted fusions. *Semin. Cell Dev. Biol.* **22,** 866–874 (2011).
3. Lee, J. A., Carvalho, C. M. & Lupski, J. R. A. DNA replication mechanism for generating nonrecurrent rearrangements associated with genomic disorders. *Cell* **131,** 1235–1247 (2007).
4. San Filippo, J., Sung, P. & Klein, H. Mechanism of eukaryotic homologous recombination. *Annu. Rev. Biochem.* **77,** 229–257 (2008).
5. Wu, L. & Hickson, I. D. The Bloom's syndrome helicase suppresses crossing over during homologous recombination. *Nature* **426,** 870–874 (2003).
6. Schlacher, K. *et al.* Double-strand break repair-independent role for BRCA2 in blocking stalled replication fork degradation by MRE11. *Cell* **145,** 529–542 (2011).
7. Schlacher, K., Wu, H. & Jasin, M. A distinct replication fork protection pathway connects Fanconi anemia tumor suppressors to RAD51-BRCA1/2. *Cancer Cell* **22,** 106–116 (2012).
8. Mizuno, K., Lambert, S., Baldacci, G., Murray, J. M. & Carr, A. M. Nearby inverted repeats fuse to generate acentric and dicentric palindromic chromosomes by a replication template exchange mechanism. *Genes Dev.* **23,** 2876–2886 (2009).
9. Mizuno, K., Miyabe, I., Schalbetter, S. A., Carr, A. M. & Murray, J. M. Recombination-restarted replication makes inverted chromosome fusions at inverted repeats. *Nature* **493,** 246–249 (2013).
10. Petermann, E., Orta, M. L., Issaeva, N., Schultz, N. & Helleday, T. Hydroxyurea-stalled replication forks become progressively inactivated and require two different RAD51-mediated pathways for restart and repair. *Mol. Cell* **37,** 492–502 (2010).
11. Carr, A. M. & Lambert, S. Replication stress-induced genome instability: the dark side of replication maintenance by homologous recombination. *J. Mol. Biol.* http://dx.doi.org/10.1016/j.jmb.2013.04.023 (30 April 2013).
12. Ulrich, H. D. Regulating post-translational modifications of the eukaryotic replication clamp PCNA. *DNA Repair (Amst.)* **8,** 461–469 (2009).
13. Falbo, K. B. *et al.* Involvement of a chromatin remodeling complex in damage tolerance during DNA replication. *Nature Struct. Mol. Biol.* **16,** 1167–1172 (2009).
14. Huang, J. *et al.* RAD18 transmits DNA damage signalling to elicit homologous recombination repair. *Nature Cell Biol.* **11,** 592–603 (2009).
15. Kim, T. M. *et al.* RAD51 mutants cause replication defects and chromosomal instability. *Mol. Cell. Biol.* **32,** 3663–3680 (2012).
16. Shimizu, N., Shingaki, K., Kaneko-Sasaguri, Y., Hashizume, T. & Kanda, T. When, where and how the bridge breaks: anaphase bridge breakage plays a crucial role in gene amplification and HSR generation. *Exp. Cell Res.* **302,** 233–243 (2005).
17. Cavalli, G. & Misteli, T. Functional implications of genome topology. *Nature Struct. Mol. Biol.* **20,** 290–299 (2013).
18. Harada, S., Sekiguchi, N. & Shimizu, N. Amplification of a plasmid bearing a mammalian replication initiation region in chromosomal and extrachromosomal contexts. *Nucleic Acids Res.* **39,** 958–969 (2011).
19. Horvath, J. E. *et al.* Using a pericentromeric interspersed repeat to recapitulate the phylogeny and expansion of human centromeric segmental duplications. *Mol. Biol. Evol.* **20,** 1463–1479 (2003).
20. Luo, G. *et al.* Cancer predisposition caused by elevated mitotic recombination in Bloom mice. *Nature Genet.* **26,** 424–429 (2000).
21. Motegi, A. *et al.* Polyubiquitination of proliferating cell nuclear antigen by HLTF and SHPRH prevents genomic instability from stalled replication forks. *Proc. Natl Acad. Sci. USA* **105,** 12411–12416 (2008).
22. Tateishi, S. *et al.* Enhanced genomic instability and defective postreplication repair in *RAD18* knockout mouse embryonic stem cells. *Mol. Cell. Biol.* **23,** 474–481 (2003).
23. Chen, M. J., Ma, S. M., Dumitrache, L. C. & Hasty, P. Biochemical and cellular characteristics of the 3′ → 5′ exonuclease TREX2. *Nucleic Acids Res.* **35,** 2682–2694 (2007).
24. Dumitrache, L. C., Hu, L. & Hasty, P. TREX2 exonuclease defective cells exhibit double-strand breaks and chromosomal fragments but not Robertsonian translocations. *Mutat. Res.* **662,** 84–87 (2009).
25. Chen, M. J. *et al.* Cisplatin depletes TREX2 and causes Robertsonian translocations as seen in TREX2 knockout cells. *Cancer Res.* **67,** 9077–9083 (2007).
26. Dumitrache, L. C. *et al.* Trex2 enables spontaneous sister chromatid exchanges without facilitating DNA double-strand break repair. *Genetics* **188,** 787–797 (2011).
27. Goldfless, S. J., Morag, A. S., Belisle, K. A., Sutera, V. A. Jr & Lovett, S. T. DNA repeat rearrangements mediated by DnaK-dependent replication fork repair. *Mol. Cell* **21,** 595–604 (2006).
28. Dutra, B. E. & Lovett, S. T. *Cis* and *trans*-acting effects on a mutational hotspot involving a replication template switch. *J. Mol. Biol.* **356,** 300–311 (2006).
29. Sirbu, B. M. *et al.* Analysis of protein dynamics at active, stalled, and collapsed replication forks. *Genes Dev.* **25,** 1320–1327 (2011).
30. Blastyák, A., Hajdú, I., Unk, I. & Haracska, L. Role of double-stranded DNA translocase activity of human HLTF in replication of damaged DNA. *Mol. Cell. Biol.* **30,** 684–693 (2010).

Acknowledgements We thank C. Williams and S. Dodds for technical assistance and the Molecular Cytogenetic Core at Albert Einstein College of Medicine for help with the execution of spectral karyotyping and two-colour FISH. This work was supported by the National Institutes of Health (1 RO1 CA123203-01A1 to P.H., 2P01AG017242-12 to P.H. and C.M. P30CA013330 to C.M.) and with support from the Cancer Therapy & Research Center at The University of Texas at San Antonio (CTRC) (P30 CA054174).

Author Contributions L.H., T.M.K., P.R.Y., C.M., L.C.D. and P.H. designed experiments and interpreted results. L.H., T.M.K., M.Y.S., S.-AK., C.L.H., D.H.K. and PH performed experiments. S.T. provided the *rad18*$^{-/-}$ and IB10 ES cells. P.H. wrote the paper with comments from the other authors.

Author Information Reprints and permissions information is available at www.nature.com/reprints. The authors declare no competing financial interests. Readers are welcome to comment on the online version of the paper. Correspondence and requests for materials should be addressed to P.H. (hastye@uthscsa.edu).

METHODS

Construction of the IRR and MRR. The IRR and MRR contain a puromycin phosphotransferase (puro) selection cassette and an *HPRT* minigene[31] (*miniHPRT*). Puro was positioned 5′ to *miniHPRT* and used to select for stable transfectants. *MiniHPRT* contains a phosphoglycerate kinase 1 (PGK) promoter[32], exons 1 and 2, intron and exons 3–8 with polyadenylation sequences. The 3′ half of *miniHPRT* was inverted from intronic XbaI. Major satellite repeats (MSRs)[33] were positioned at inversion junctions in an indirect orientation. The same MSR sequence (below) is located at both junctions for the IRR (Fig. 1a, green arrow) and at the 5′ junction for the MRR (Fig. 1b, green arrow) while a divergent MSR (seven mismatches) is located at the 3′ end for the MRR (Fig. 1b, orange arrow). These mismatches are the only difference between the reporters.

MSR sequence, mismatched nucleotides underlined (Fig. 1a, b, green arrow):

5′-TGGAATATGGCGAGAAAACTGAAAATCATGGAAAATGAGAAATA CACACTTCAGGACGTGAAATATGGCGAGGAAAACTGAAAAAGGTGGAA AATTTAGAAATGTCCACTGTAGGACGTGGAATATGGCAAGAAAACTGT-AAATCATGGAAAATGAGAAACATCCACTTGACGACTTGAAAAATGACA-AAATCACTAAAAAACATGAAAAATGAGAAATGCACACTGAAGGACCTG GAATATGGCTAGAAAACTGAAAATCACGGAAAATGAGAAATACAAA CCTTAGGACTTGAAATATGGCGAGGAAAACT3′

MSR sequence, mismatched nucleotides are underlined (Fig. 1b, orange arrow)

5′-TGGAATATGGCGAGAAAACTGAAAATCATGGAAAATGAGAAATA CACACTTTAGGACGTGAAATATGGCGAGGAAAACTGAAAAAGGTGGA AAATTTAGAAATGTCCACTTTAGGACGTGGAATATGGCAAGAAAACT-GAAAATCATGGAAAATGAGAAACATCCACTTGACGACTTCAAAAATG-ACGAAATCACTAAAAAACGTGAAAAATGAGAAATGCACACTGAAGGA CCTGGAATATGGCGAGAAAACTGAAAATCACGGAAAATGAGAAATAC AAACCTTAGGACTTGAAATATGGCGAGGAAAACTG-3′

PCR amplification of repeat fusion. PCR amplify fusions with primers 5′ (HPRT4) and 3′ (HPRT recom Rev) to XbaI. Sequence PCR products with the same primers.

HPRT4, 5′-TCTCAAGCACTGGCCTATGC 3′; HPRT recom Rev, 5′-AGA CAGAATGCTATGCAACC-3′.

Conditions: 1 cycle at 98 °C for 10 min, 35 cycles: 98 °C for 1 min, 62 °C for 1 min, 72 °C for 20 s.

Tissue culture for mouse ES cells. Maintain ES cells in M15 (high glucose DMEM with 15% fetal bovine serum, 100 μM β-mercaptoethanol, 2 mM L-glutamine, 3 mg ml^{-1} penicillin, 5 mg ml^{-1} streptomycin, 1,000 U ml^{-1} ESGRO (LIF)) on plastic plates precoated with gelatin (0.1%, ~1 h) and seeded with 2.5 × 10^6 primary murine embryonic fibroblasts (MEFs, mutated for *Hprt* and resistant to puromycin, exposed to 30 Gy γ-irradiation) and incubate at atmospheric O_2, 5% CO_2, 37 °C. ES cells were also cultured on gelatinized plates without feeders.

Repeat fusion assay. Repeat fusion is seen in cells transfected with the IRR or MRR (Figs 1d, 2 and 3b). Transfect ES cells (5 × 10^6, 800 μl PBS) with 5 μg of uncut IRR or MRR by electroporation (Bio-Rad Gene Pulsar at 230 V, 500 μF). Seed cells onto 3–6 3.5-cm plates with mitotically inactivated MEFs. Each well is a replicate because they remain separate. Add puromycin (3 μg ml^{-1}) next day. About 100–200 puromycin resistant colonies grow for each well. Seven days later, pool puromycin-resistant colonies for each well and passage onto a 3.5-cm plate precoated with gelatin. Three days later passage cells onto a 10-cm plate precoated with gelatin. See below for cell exposure to DNA-damaging agents. For unexposed cells, next day seed 10^6 cells onto a gelatin-coated 10-cm plastic plate in M15 supplemented with 1× HAT (1 mM sodium hypoxanthine, 4 μM aminopterin and 160 μM thymidine). Count HAT-resistant colonies 10 days later. To control for seeding efficiencies, seed 2,000 cells for each replicate onto a gelatin-coated 3.5-cm plastic plate and culture in M15 without selection. Determine percentage of HAT-resistant colonies by dividing the number of HAT-resistant colonies by the number of cells electroporated multiplied by the seeding efficiency.

For cells exposed to DNA-damaging agents (γ-radiation or ultraviolet light or hydroxyurea (HU)) the protocol is the same for the transfection, selection in puromycin and expansion of puromycin resistant cells (see earlier). After expansion, expose cells to either 4 Gy γ-radiation (^{137}Cs at a rate of 0.125 Gy s^{-1}, Mark1 gamma radiation source from Shepard and Associates) or 20 J m^{-2} ultraviolet light (a dual wavelength ultraviolet transilluminator from Alpha Innotech at a rate of 1 J m^{-2} s^{-1}) or HU (0.5 mM, 90 min). For γ-radiation and ultraviolet light, expose cells directly on the plate after removing media. Then add 10 ml of pre-warmed (37 °C) fresh media and incubated for 48 h. Then seed 10^6 cells onto a gelatin-coated 10-cm plastic plate in M15 supplemented with 1× HAT. Count HAT-resistant colonies 10 days later. To control for seeding efficiencies and survival fraction, seed 2,000 cells for each replicate onto a gelatin-coated 3.5-cm plastic plate and culture in M15 without selection. Survival fraction is ~10%, 0.6% or 100% after exposure to γ-radiation (4 Gy), ultraviolet (20 J m^{-2}) or HU (0.5 mM, 90 min), respectively.

Two-colour FISH with the pericentromeric and telomeric probes. Perform two-colour FISH (Extended Data Fig. 2a) on HAT-resistant colonies expanded with the IRR or MRR. Seed cells in HAT selection media on plastic plates pre-coated with gelatin. Next day add fresh media (without HAT). Treat cells with colcemid (540 nM, 4 h) then trypsinize. Slide preparation: spin cells (180*g*, for 10 min), wash twice in PBS (pH 7.4) and resuspend pellet in 300 μl 75 mM KCl, drop-wise, flicking tube. Incubate in a 37 °C water bath (15 min). Add drop-wise 300 μl methanol/acetic acid (2:1 fixative) while flicking tube, spin 845*g*, 30 s. Wash cells in 300 μl 2:1 fixative, drop-wise, flicking tube, spin 850*g*, 30 s; repeat wash. Hybridization: place slides in methanol overnight, then incubate in 70% formamide at 70 °C, place slides in 30% formamide at 37 °C in dark with 500 μl per slide of 0.25 mg ml^{-1} pericentromeric (CY-3 5′-TGGAATATGGCGAGAAAACTGA AAATCATGGAAAATGAGA-3′) and telomeric (6-FAM 5′-(CCCTAA)$_7$ 3′) probes for 15 min, wash in PBS, 10 dips, coverslip in 4′,6-diamidino-2-phenylindole (DAPI).

Spectral karyotyping. Perform spectral karyotyping (Fig. 1f) as described[34] with commercial spectral karyotyping paint probes from Applied Spectral Imaging. Define rearrangements with nomenclature rules from the International Committee on Standard Genetic Nomenclature for Mice[35].

Two-colour FISH with the MRR and chromosome 1 or 14 paint. Perform two-colour FISH (Extended Data Fig. 2b) with custom-made chromosome paint probes specific for murine autosomes 1 and 14 labelled with the Spectrum Green (Dyomics) using a standard degenerate oligonucleotide primed-polymerase chain reaction (DOP-PCR) protocol (http://atlasgeneticsoncology.org/Deep/ComparCancerCytogID20011.html). Label MRR with Spectrum Orange dUTP (Dyomics) by nick-translation and hybridize to chromosomal preparations derived from clone 18 (Extended Data Table 3). After overnight hybridization (37 °C), wash slides and counterstain with DAPI and image random fields with an inverted Zeiss Axiovert 200 using fine focusing oil immersion lens (×60, numerical aperture 1.35). Equip microscope with a Camera Hall 100 and Applied Spectral Imaging software.

Generation of mouse *Rad51* targeting vector. Construct mouse *Rad51* targeting vector (Extended Data Fig. 3) as described[36]. Amplify left (5′) and right (3′) homologous arms with high-fidelity PCR using genomic DNA extracted from AB2.2 ES cells and iProof DNA polymerase (Bio-Rad Laboratories) in 25 μl containing 5 μl of 5× iProof HF buffer, 0.5 μl of 10 mmol l^{-1} deoxynucleotide triphosphates, 0.75 μl of 4 μmol l^{-1} forward and reverse primers (below), 100 ng of genomic DNA, and 0.25 μl of iProof DNA polymerase.

Left arm primers: Rad51KiLA forward, 5′-CACACTCGAGTCCCCTCTA CGCTGAGAAGCCGGAGAAAG-3′; Rad51KiLA reverse, 5′-CACAGCGGCCG CAGGCCACTAAGGCCAGAACTGCAGCTGGCCCTCCCTATCCAC-3′.

Right arm primers: Rad51KiRA forward, 5′-CACAGCGGCCGCAGGCCT GCGTGGCCGGATTATAGGAATGTCAGCTTCTCATAGAC-3′; Rad5KiRA reverse, 5′-CACAGTCGACGGTACTGGTTAGTTCATAATGTTGTTCCA-3′.

PCR conditions for both arms: 1 cycle: 98 °C for 5 min 35 cycles: 98 °C for 1 min, 64.7–70.2 °C gradient for 1 min, 72 °C for 1 min and 30 s. 1 cycle: 72 °C for 10 min.

After amplifying arms, digest left arm (3.9 kb) with SalI and NotI and clone into a plasmid backbone, pKO, cut with XhoI and NotI. Then, digest right arm (3.0 kb) with XhoI and NotI and clone into the same backbone digested with SalI and NotI to delete *Rad51* exons 2–4. Then, clone floxed SAβgeo-*miniHPRT* (Extended Data Fig. 3a) into unique SfiI sites as described[36].

Transfect targeting vector (5 μg, cut with PacI) into *blm*$^{-/-}$ ES cells (5 × 10^6 cells in 800 μl PBS) by electroporation (Gene Pulser Cuvettes with a 0.4 cm electrode gap at 230 V, 500 μF with a Gene Pulser Apparatus from Bio-Rad). After electroporation, seed cells onto two 10 cm plates with mitotically inactive MEFs. Next day, add M15 medium containing 1× HAT (0.1 mM hypoxanthine, 0.0004 mM aminopterin and 0.016 mM thymidine). Pick HAT-resistant colonies 7 days later onto a 96-well plate and maintain in HAT selection. Replica plate to freeze one plate and use the other to isolate genomic DNA[37]. Screen for targeted clones with PCR (Extended Data Fig. 3b).

H13F (in *miniHPRT*): 5′-GTAAATGAAAAAATTCTCTTAAACCACAGCA CTATTGAG-3′ SR3 (outside the right arm): 5′-AGCCAGGTATAGTCTCAAA GGAATCTGCAATCC-3′.

PCR conditions: 1 cycle: 98 °C for 5 min; 35 cycles: 98 °C for 1 min, 67 °C for 1 min, 72 °C for 1 min 30 s; and 1 cycle: 72 °C for 10 min.

Cre-mediated deletion of SAβgeo and 5′ *miniHPRT*. Delete *SAβgeo* and 5′ half of *miniHPRT* using Cre recombinase to generate *Rad51*$^{+/\Delta ex2\text{-}4}$ cells (Extended Data Fig. 3c). Expand targeted ES cells in 1× HAT to remove HPRT-negative cells that survive due to cross feeding. Removed HAT selection 2 days before transfection and cultured in 1× HT (1 mM sodium hypoxanthine and 160 μM thymidine); electroporate 5 × 10^6 cells in 800 μl DPBS with 10 μg of pPGKcrepA using a Bio-Rad Gene Pulsar at 230 V, 500 μF. After electroporation, seed 200 μl onto a 10-cm feeder plate without selection for 2–4 days to allow time for *miniHPRT* removal

and time for degradation of *HPRT* mRNA and protein. Then seed 4×10^4 cells onto a 10-cm feeder plate in 10 μM 6-thioguanine. Pick 6-thioguanine-resistant colonies 10 days later. Expand cells in 10 μM 6-thioguanine and replica plate. Freeze one plate and use the other to isolate genomic DNA[37]. Confirmed Cre-mediated deletion with PCR (1.4 kb fragment).

PCR primers. RCF1 (in *RAD51* intron 1), 5′-GTGCTGAATCTCCTAGAA CTG-3′; AS2 (in exon cluster 3-8 of *miniHPRT*), 5′-TGTCCCCTGTTGACTGG TCA-3′.

PCR conditions: 1 cycle: 98 °C for 5 min, 35 cycles: 98 °C for 1 min, 64 °C for 1 min, 72 °C for 30 s. 1 cycle: 72 °C for 10 min.

Targeting mouse *Brca2* exon 27. Replace the first copy of *Brca2* exon 27 with PGKneobpA[38] by cloning PGKneobpA into the Sfi1 sites of the *Brca2* exon 27 deletion targeting vector (Extended Data Fig. 4a)[36]. Transfect as described for *Rad51*. Use PCR to detect targeted clones (Extended Data Fig. 4a).

PCR primers: NF (in neo), 5′-AGCGCATCGCCTTCTATCGCCTTCTTG ACG-3′; *Brca2* intron 27 reverse, 5′-CCCCGTCGACCGGAGAGCTAATGG CCTCTACTCCAACG-3′. Conditions: 35 cycles of 98 °C for 1 min, 65 °C for 1 min, 72 °C for 1 min and 30 s.

Replace the second copy of *Brca2* exon 27 with floxed *miniHPRT* (Extended Data Fig. 4b)[36]. Use PCR to detect targeted clones (Extended Data Fig. 4b).

PCR primers: H13F, 5′-GTAAATGAAAAAATTCTCTTAAACCACAGC ACTATTGAG-3′; B27R, 5′-CCCCGTCGACCGGAGAGCTAATGGCCTCTAC TCCAACG-3′. Conditions: 35 cycles of 98 °C for 1 min, 65 °C for 1 min, 72 °C for 1 min and 30 s.

Removed the 5′ half of *miniHPRT* by Cre-mediated recombination[36] to generate $Brca2^{\Delta ex27\text{-}h/\Delta ex27\text{-}n}$ cells. Use PCR to detect removal (Extended Data Fig. 4b).

PCR primers: Bi26, 5′-TCAATCAAGCAGTCCTCACC-3′; H3-8R: 5′-TGACCAGTCAACAGGGGACA-3′. Conditions: 35 cycles: 98 °C for 1 min, 65 °C for 1 min, 72 °C for 45 s.

Coimmunoprecipitation of IdU and Myc-TREX2 after exposure to ultraviolet light. TREX2 associates with nascent strand DNA after ultraviolet exposure (Extended Data Fig. 5a). Experiment performed as described[10] with minor modifications. Transfected HeLa cells with 5 μg Myc-TREX2 using FuGENE6 (Roche). Label cells with IdU (5 μM, 30 min), treat with 20 J m^{-2} ultraviolet and recover with the indicated time. Crosslink cells in formaldehyde (1%, 15 min 24 °C). Remove cytoplasmic protein fraction by incubation in hypotonic buffer (10 mM HEPES, 1.5 mM $MgCl_2$, 10 mM KCl, β-mercaptoethanol, PMSF, Protease Inhibitor (Roche) for 10 min on ice). Resuspend pellets in nuclear exact buffer (20 mM HEPES, 20% glycerol, 400 mM KCl, 1.5 mM $MgCl_2$, 0.2 mM EDTA, β-mercaptoethanol, PMSF, Protease Inhibitor (Roche)). Dilute nuclear exact protein (50 μg) solution with equal volume of immunoprecipitation dilution buffer (20 mM HEPES, 0.2 mM EDTA, 10% glycerol, PMSF, Protease Inhibitor (Roche)) and pre-wash with Protein G Sepharose beads (10 μl, 1 h). Remove bead and immunoprecipitate supernatant by incubating with 1 μg of anti-BrdU (mouse anti-BrdU B44) at 4 °C overnight. Incubate reaction solution with 20 μl Protein G Sepharose beads for 3 h at 4 °C and wash beads 4 times with immunoprecipitation wash buffer. Separate immunoprecipitated proteins with SDS–PAGE gel and blot with anti-Myc (BD Bioscience) antibody.

TREX2-UBC13 association. TREX2 associates with UBC13 by GST pull-down (Extended Data Fig. 5b). Bind GST–MMS2, GST–UBC13, and GST–TREX2 fusion proteins (5 μg) to glutathione–Sepharose 4B (GE Healthcare) and incubate with [^{35}S]methionine-labelled TREX2 (4 μl, 1.5 h, 23 °C)[39]. Wash beads with NETN buffer (50 mM Tris, 250 mM NaCl, 5 mM EDTA, pH 7.5, and 0.1% NP40) and subject to SDS–PAGE and phosphorimager analysis.

TREX2 associates with UBC13 by coimmunoprecipitation in HeLa cells (Extended Data Fig. 5c). Transfect HeLa cells with 5 μg Myc-TREX2 and 5 μg HA-UBC13 plasmid (48 h) using FuGENE6 (Roche), expose cells to 0 J m^{-2} or 20 J m^{-2} ultraviolet as described for the PCNA ubiquitination assay (below). Crosslink cells in formaldehyde (1%, 15 min, 24 °C). Incubate in hypotonic buffer (10 mM HEPES, 1.5 mM $MgCl_2$, 10 mM KCl, β-mercaptoethanol, PMSF, Protease Inhibitor (Roche)) for 10 min on ice to remove cytoplasmic protein fraction. Resuspend pellets in nuclear exact buffer (20 mM HEPES, 20% glycerol, 400 mM KCl, 1.5 mM $MgCl_2$, 0.2 mM EDTA, β-mercaptoethanol, PMSF, Protease Inhibitor (Roche)). Dilute nuclear exact protein (50 μg) solution with equal volumes of immunoprecipitation dilution buffer (20 mM HEPES, 0.2 mM EDTA, 10% glycerol, PMSF, Protease Inhibitor (Roche)) and incubate with 10 μl Protein G Sepharose beads (1 h). Remove beads and immunoprecipitate supernatant by incubating with 2 μg anti-Myc (BD Bioscience) or anti-HA (Roche) antibody at 4 °C overnight. Incubate reaction solution with 20 μl Protein G Sepharose beads for 3 h. Wash beads 4 times with immunoprecipitation wash buffer. Separate immunoprecipitated proteins by SDS–PAGE gel and blot with anti-Myc or anti-HA antibody.

Detection of PCNA ubiquitination with chromatin-bound fraction. RAD18 and TREX2 participated in ultraviolet-induced PCNA ubiquitination (Extended Data Fig. 6). Isolate chromatin-bound fraction as described[21,40] with modifications. Briefly, resuspend ~1.5×10^7 cells in buffer A (10 mM HEPES (pH 7.9), 1.5 mM $MgCl_2$, 10 mM KCl, 0.34 M sucrose, 10% glycerol, 0.1% Triton X-100 and protease inhibitor cocktail (Roche)), incubate and rotate 5 min at 4 °C then centrifuge (5,204*g*, 2 min, 4 °C). Remove soluble fraction. Resuspended pellet in buffer then centrifuge (5,204*g*, 3 min, 4 °C). Extract chromatin-bound fraction, resuspend pellet in buffer B (20 mM Tris-Cl (pH 8.1), 2 mM EDTA (pH 8.0), 500 mM NaCl, 0.1% SDS, 1% Triton X-100 and protease inhibitor cocktail (Roche)), sonicate, treat with micrococcal nuclease (10 min, 37 °C) and centrifuge (17,948*g*, 15 min, 4 °C). Immunoprecipitate supernatant containing released chromatin-bound protein. Pre-incubate with protein G Sepharose beads (GE healthcare) (1–2 h, 4 °C) to pre-cleaned protein and incubated with 1 μg of anti-PCNA antibody (PC10, Santa Cruz Biotechnology) overnight at 4 °C. Precipitate anti-PCNA immune complexes with 30 μl protein G Sepharose beads for 3 h at 4 °C). Separate protein on 10% SDS–PAGE gel and transfer onto PVDF membrane. Use monoclonal antibodies for western blot: anti-ubiquitin (P4D1, COVANCE; 1:1,000–2,000) or anti-PCNA (PC10, Santa Cruz Biotechnology; 1:2,000–2,500). Used mouse TrueBlot ULTRA (Anti-mouse Ig HRP, ROCKLAND; 1:1,000–2,500) to minimize IgG signal. Quantify band intensities with ImageJ software (http://rsbweb.nih.gov/ij/).

Targeting *Trex2* in IB10 cells and $rad18^{-/-}$ cells. Electroporate *Trex2* targeting vector (5 μg of PacI-cut) (Extended Data Fig. 7)[25] into IB10 cells and $rad18^{-/-}$ cells as described for *Rad51*.

Primers to detect left arm integration: TX2 LR55 (outside of left arm), 5′-TATATTTAGGAGACAAAGTGGCCCTGCCAGAGCTG-3′; HATrev (in the *HPRT* minigene), 5′-CATGCGCTTTAGCAGCCCCGCTGGGCACTTGGCGC-3′. Conditions: 1 cycle: 98 °C for 5 min 35 cycles: 98 °C for 1 min, 72 °C for 1 min, 72 °C for 2 min 30 s. 1 cycle: 72 °C for 10 min.

Primers to detect right arm integration: HATfor (in the *HPRT* minigene), 5′-GTAAATGAAAAAATTCTCTTAAACCACAGCACTATTGAG-3′; TX2 RR33 (outside the right arm), 5′-CCTGTTTCACAAATATCAGGACCTGAGTTT GTATCC-3′. Conditions: 1 cycle: 98 °C for 5 min 35 cycles: 98 °C for 1 min, 63.5 °C for 1 min, 72 °C for 2 min 30 s. 1 cycle: 72 °C for 10 min.

Primers to confirm deletion of TREX2 open reading frame: mTX2For, 5′-AAAAGAATTCCCGCCACCATGTCTGAGCCACCCCGGGC-3′; mTX2Rev: 5′-AAAACTCGAGTCAGGCTTCGAGGCTTGGACC-3′. Conditions: 1 cycle: 98 °C for 5 min 35 cycles: of 98 °C for 1 min, 65 °C for 1 min, 72 °C for 25 min. 1 cycle: 72 °C for 10 min.

Microfibre analysis. RAD18 and TREX2 enabled replication fork restart (Fig. 3a). Perform DNA fibre analysis as described[10,15] with modifications. Pulse-label ES cells with IdU (25 μM, 20 min), wash twice with medium, expose to HU (0.5 mM, 1.5 h), wash twice with medium and pulse-label with CldU (250 μM, 20 min). Fix fibres in methanol and acetic acid (3:1) and air-dry. To denature fibres, treat slides with HCl (2.5 M, 75–80 min) and wash twice with PBS then block 1 h with 1% BSA (bovine serum albumin) + 0.1% Tween 20. Incubate slides with primary antibodies against CldU (rat anti-BrdU BU1/75[ICR1], Abcam, 1:1,000) and IdU (mouse anti-BrdU B44, 1:750) for 1.5 h. Fix slides with 4% paraformaldehyde and wash thrice with PBS. Apply AlexaFluor 555-conjugated goat anti-rat IgG (Molecular Probes, 1:500) and AlexaFluor 488-conjugated goat anti-mouse IgG (Molecular Probes, 1:500) to slides for 2 h. Wash slides and mount in Fluoroshield (Sigma) and examine (Axioplan2, Zeiss fluorescent microscope).

Statistics. Student's *t*-test was used for statistics (two-sided without adjustments for multiple comparisons). The average was the centre value. In all figures the s.e.m. is shown and the number of biological replicates are provided in the legends.

31. Reid, L. H., Gregg, R. G., Smithies, O. & Koller, B. H. Regulatory elements in the introns of the human HPRT gene are necessary for its expression in embryonic stem cells. *Proc. Natl Acad. Sci. USA* **87,** 4299–4303 (1990).
32. Adra, C. N., Boer, P. H. & McBurney, M. W. Cloning and expression of the mouse *pgk-1* gene and the nucleotide sequence of its promoter. *Gene* **60,** 65–74 (1987).
33. Guenatri, M., Bailly, D., Maison, C. & Almouzni, G. Mouse centric and pericentric satellite repeats form distinct functional heterochromatin. *J. Cell Biol.* **166,** 493–505 (2004).
34. Montagna, C., Andrechek, E. R., Padilla-Nash, H., Muller, W. J. & Ried, T. Centrosome abnormalities, recurring deletions of chromosome 4, and genomic amplification of HER2/*neu* define mouse mammary gland adenocarcinomas induced by mutant HER2/*neu*. *Oncogene* **21,** 890–898 (2002).
35. Davisson, M. T. Rules and guidelines for nomenclature of mouse genes. *Gene* **147,** 157–160 (1994).
36. Holcomb, V. B. *et al. HPRT* minigene generates chimeric transcripts as a by-product of gene targeting. *Genesis* **45,** 275–281 (2007).
37. Ramírez-Solis, R. *et al.* Genomic DNA microextraction: a method to screen numerous samples. *Anal. Biochem.* **201,** 331–335 (1992).
38. Soriano, P., Montgomery, C., Geske, R. & Bradley, A. Targeted disruption of the c-src proto-oncogene leads to osteopetrosis in mice. *Cell* **64,** 693–702 (1991).
39. Kim, D. H. *et al.* The $CRL4^{Cdt2}$ ubiquitin ligase mediates the proteolysis of cyclin-dependent kinase inhibitor Xic1 through a direct association with PCNA. *Mol. Cell. Biol.* **30,** 4120–4133 (2010).

40. Krijger, P. H. *et al.* HLTF and SHPRH are not essential for PCNA polyubiquitination, survival and somatic hypermutation: existence of an alternative E3 ligase. *DNA Repair (Amst.)* **10,** 438–444 (2011).
41. Friedrich, G. & Soriano, P. Promoter traps in embryonic stem cells: a genetic screen to identify and mutate developmental genes in mice. *Genes Dev.* **5,** 1513–1523 (1991).
42. Araki, K., Araki, M. & Yamamura, K. Targeted integration of DNA using mutant lox sites in embryonic stem cells. *Nucleic Acids Res.* **25,** 868–872 (1997).
43. Kim, T. M., Choi, Y. J., Ko, J. H. & Hasty, P. High-throughput knock-in coupling gene targeting with the *HPRT* minigene and Cre-mediated recombination. *Genesis* **46,** 732–737 (2008).
44. Donoho, G. *et al.* Deletion of *Brca2* exon 27 causes hypersensitivity to DNA crosslinks, chromosomal instability, and reduced life span in mice. *Genes Chromosom. Cancer* **36,** 317–331 (2003).
45. Morimatsu, M., Donoho, G. & Hasty, P. Cells deleted for Brca2 COOH terminus exhibit hypersensitivity to gamma- radiation and premature senescence. *Cancer Res.* **58,** 3441–3447 (1998).
46. Moynahan, M. E., Pierce, A. J. & Jasin, M. BRCA2 is required for homology-directed repair of chromosomal breaks. *Mol. Cell* **7,** 263–272 (2001).
47. Terai, K., Abbas, T., Jazaeri, A. A. & Dutta, A. $CRL4^{Cdt2}$ E3 ubiquitin ligase monoubiquitinates PCNA to promote translesion DNA synthesis. *Mol. Cell* **37,** 143–149 (2010).

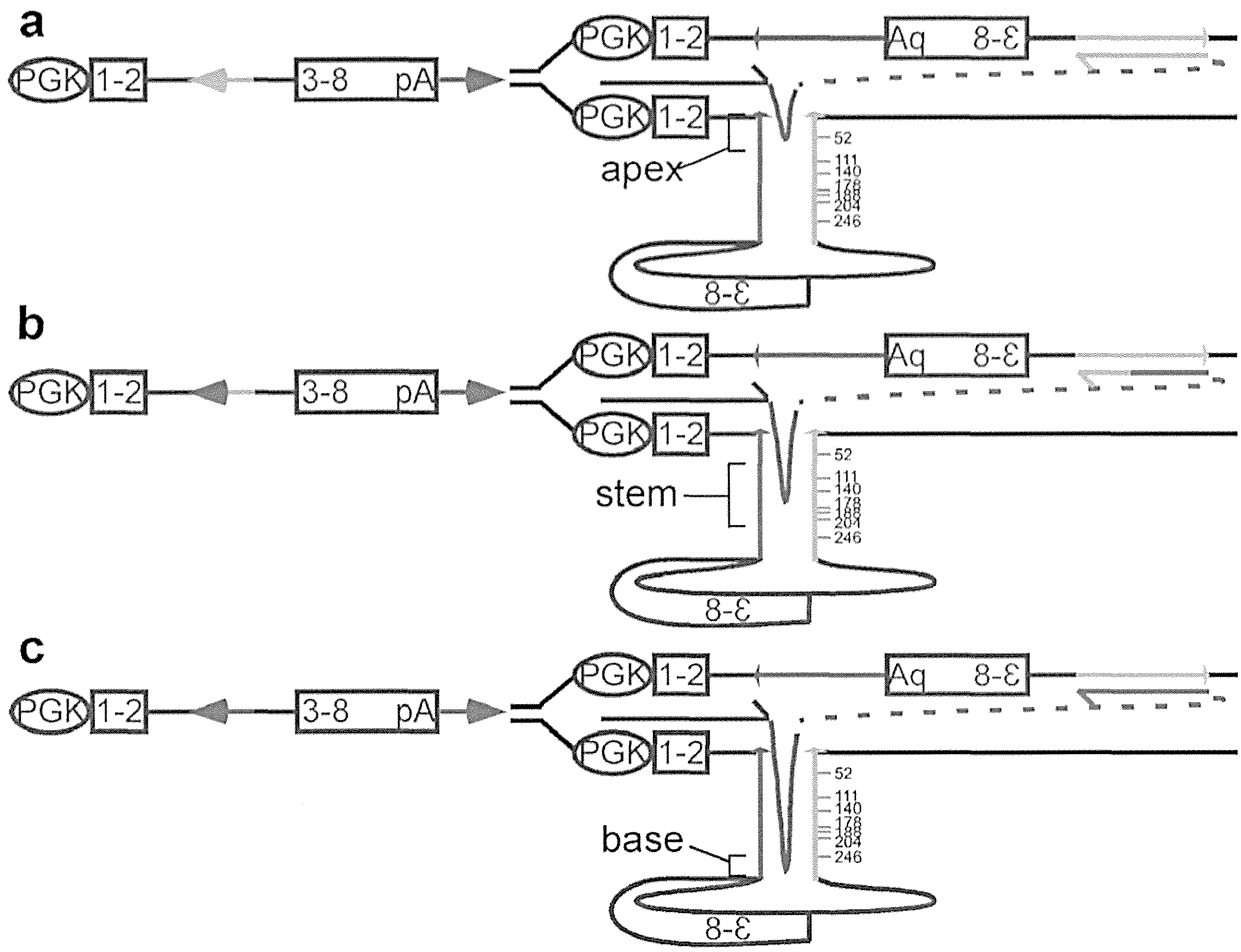

Extended Data Figure 1 | Three locations for the switch within a hairpin. There are seven mismatches located at positions 52, 111, 140, 178, 188, 204 and 246. This model shows the inverted repeats forming a hairpin to simply illustrate the location of the switch, although we do not know if hairpins form. **a**, The switch occurs at the apex of the hairpin before the first mismatch at position 52 such that the 5′ MSR has the same sequence as the orange repeat. **b**, The switch occurs in the stem of the hairpin after the first mismatch at position 52 but before the last mismatch at position 246 such that the 5′ MSR is a mixture of both the green and orange repeat. **c**, The switch occurs at the base of the hairpin after the last mismatch in position 246 such that the 5′ MSR has the same sequence as the green repeat.

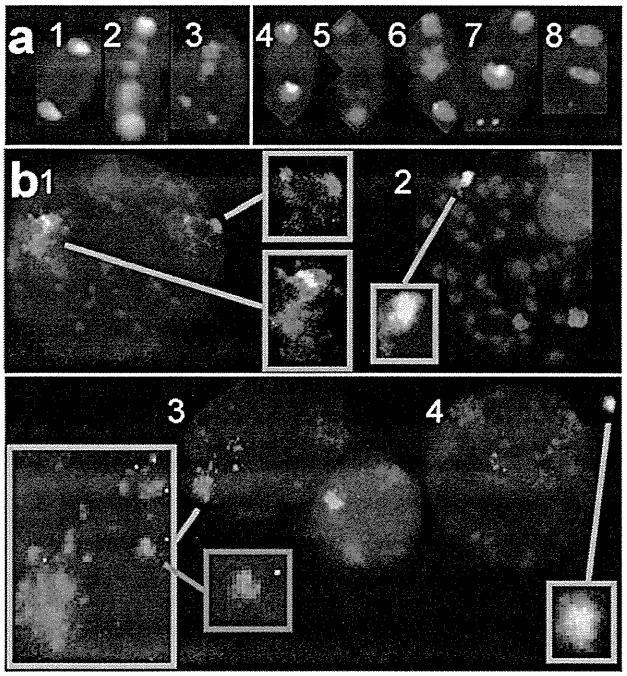

Extended Data Figure 2 | Complex chromosomal rearrangements in wild-type cells with the IRR and MRR. a, Two-colour FISH on metaphase spreads stained with a telomeric probe (green), a MSR probe in the pericentromere (red) and counterstained with DAPI (blue). (1)–(3) Multipericentric chromosomes from cells with the IRR: (1) Typical dipericentric, (2) chromosome with extra pericentromeres and telomeres (EPT)[15], (3) segmental duplication with the extra pericentromeres on only one chromatid. (4)–(8) Multipericentric chromosomes from cells with the MRR: (4) typical dipericentric, (5)–(7) EPTs, (8) extra pericentromere on only one chromatid. Chromosomal abnormalities were found for 15/19 ($P < 0.0001$, Yates-corrected chi-square test) and 18/19 ($P < 0.0001$) HAT-resistant colonies transfected with the IRR and MRR, respectively, but none were found for non-transfected cells as previously described[15]. **b**, Two-colour FISH on nuclei using the MRR as a probe (red) along with either chromosome 1 or 14 (green). For some nuclei the MMR associated with chromosome 14 (1) whereas for others it associated with chromosome 1 (2). Note the MRR is located to both chromosomes 14 but only one chromosome 1. Thus, the MRR moved to different altered chromosomes observed with spectral karyotyping, consistent with the notion that the MRR is the source of instability. In addition, the size of the red dot(s) varied, suggesting continuous nonallelic fusions that could expand or contract the number of MRR units. For some nuclei the MRR appeared as a discrete dot, indicating one contiguous array of reporter units (1 and 2, red insets) but for others it was speckled, suggesting arrays of MRR units were interspersed with chromosomal sequences (3, red inset). For one speckled cluster a fragment of chromosome 1 surrounded only one red dot, highlighting the complexity of this rearrangement (green inset). The MRR probe was also found protruding at the edge or outside of some nuclei, indicating these unstable structures could be extruded from the nucleus similar to micronuclei (4, red inset).

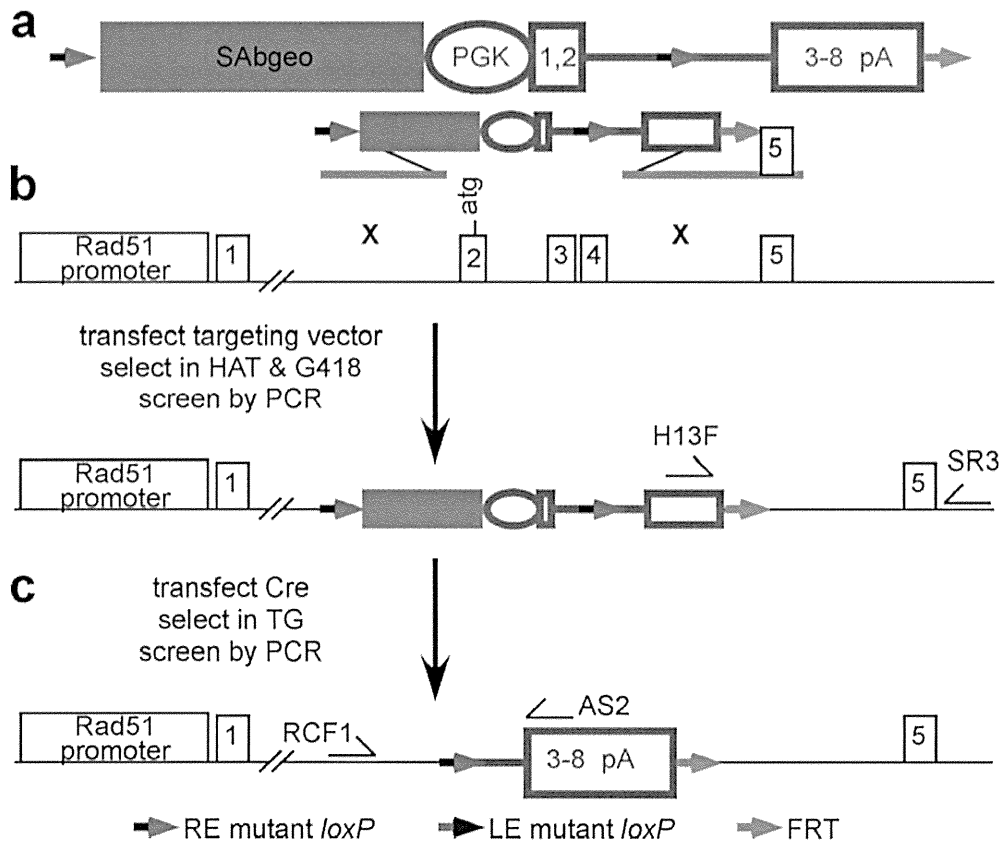

Extended Data Figure 3 | Targeting *Rad51* exons 2–4. **a**, SAβgeo-*miniHPRT* is used for selection. SAβgeo (green) is a fusion of β-galactosidase and neomycin phosphotransferase and is capable of trapping promoters to improve targeting efficiency[41]. A Right element (RE) mutant *loxP*[42] is in the intron (blue green arrow). In addition, another RE mutant *loxP* is 5′ to SAβgeo. A FLP recombination target (FRT) is at the 3′ end of *miniHPRT*[36,43]. **b**, Replacing *Rad51* exons 2–4 (exon 2 is the first coding exon) with the SAβgeo-*miniHPRT* selection cassette. PCR is used to screen G418+HAT-resistant ES cell clones for gene targeting using primers H13F and SR3. **c**, Removal of SAβgeo, the 5′ half of *miniHPRT* and a RE mutant *loxP* by Cre-mediated recombination to generate $Rad51^{+/\Delta ex2\text{-}4}$ cells. Screen 6-thioguanine-resistant clones by PCR using primers RCF1 and AS2.

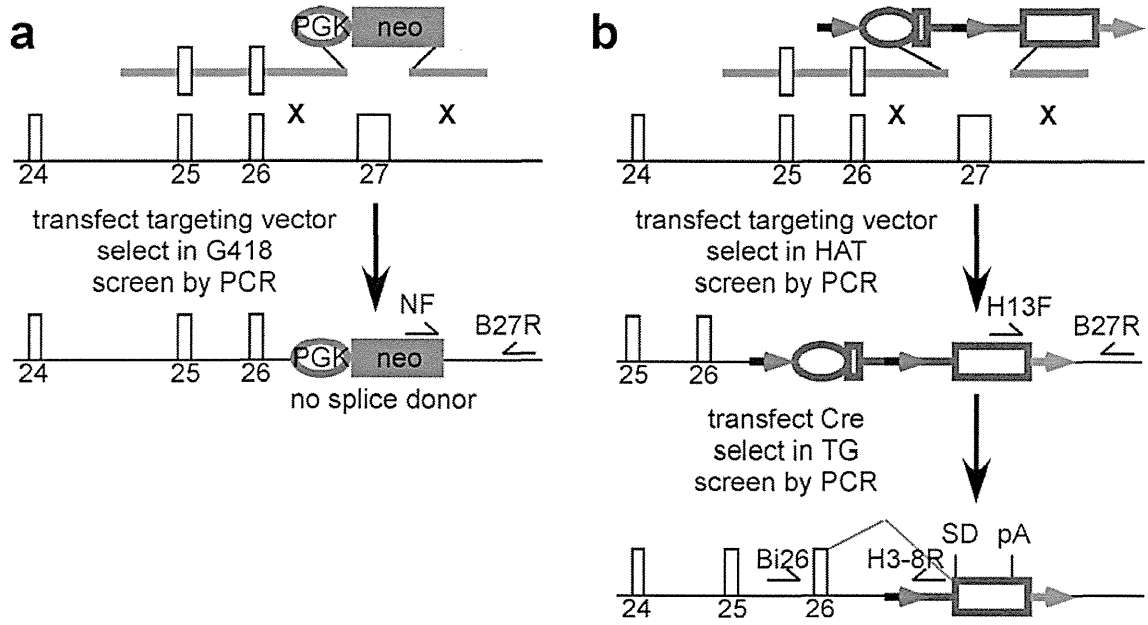

Extended Data Figure 4 | Targeting *Brca2* exon 27. There were two gene targeting vectors so we could observe cells deleted for one ($blm^{-/-}$ $Brca2^{+/\Delta ex27\text{-}n}$) and two ($blm^{-/-}$ $brca2^{\Delta ex27\text{-}h/\Delta ex27\text{-}n}$) copies of *Brca2* exon 27. **a**, The first targeting vector (Δex27-n) replaced *Brca2* exon 27 with neomycin phosphotransferase (neo) and probably generated a severe defect because exon 27 was not replaced with a splice donor to ensure polyadenylation[44]. This means deletion of the first copy probably caused a haploinsufficiency. The *Brca2* gene after targeting. NF and B27R are PCR primers used to screen for targeted clones. **b**, The second targeting vector (Δex27-h) replaced *Brca2* exon 27 with *miniHPRT* that contains a splice donor and polyadenylation sequences. Previously we showed *Brca2* exon 26 spliced into *HPRT* exon 3 to ensure polyadenylation. Cells mutated with this second targeting vector produced a truncated BRCA2 protein at normal levels and were hypersensitive to γ-radiation and deficient in homologous recombination[36,45,46] and replication fork maintenance[6]. Replacing the second copy of *Brca2* exon 27 with a floxed *miniHPRT*[36] to make $Brca2^{\Delta ex27\text{-}h/\Delta ex27\text{-}n}$ cells. H13F and B27R primers were used to screen for targeted clones. Cre-mediated recombination removed the 5′ half of *miniHPRT*. *Brca2* exon 26 splices into *miniHPRT* exons 3–8 (grey line) to generate a polyadenylated *Brca2* transcript that is deleted for exon 27[36,45]. There is the addition of one amino acid followed by a stop codon and this transcript produces a protein at wild-type levels that associates with RAD51, presumably through the BRC motifs[46]. Bi26 and H3-8R PCR primers were used to screen for Cre-mediated deletion.

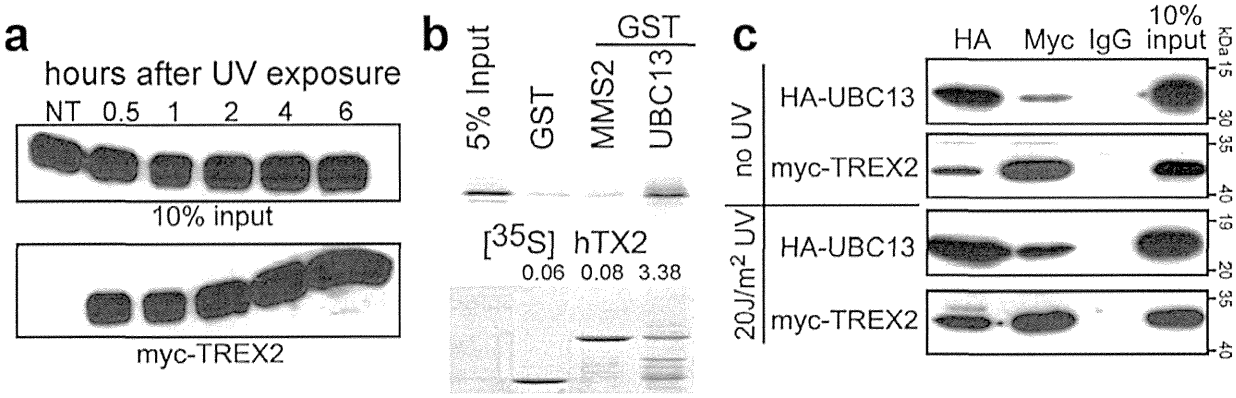

Extended Data Figure 5 | TREX2's response to ultraviolet light and association with UBC13. **a**, Coimmunoprecipitation of IdU and Myc-TREX2 in HeLa cells after exposure to 20 J m^{-2} ultraviolet light. No treatment, NT. **b**, GST pull-down of ^{35}S-labelled short isoform wild-type (WT) TREX2[23]. **c**, Coimmunoprecipitation with Myc-TREX2 and HA-UBC13 in HeLa cells before and 6 h after exposure to 20 J m^{-2} ultraviolet light.

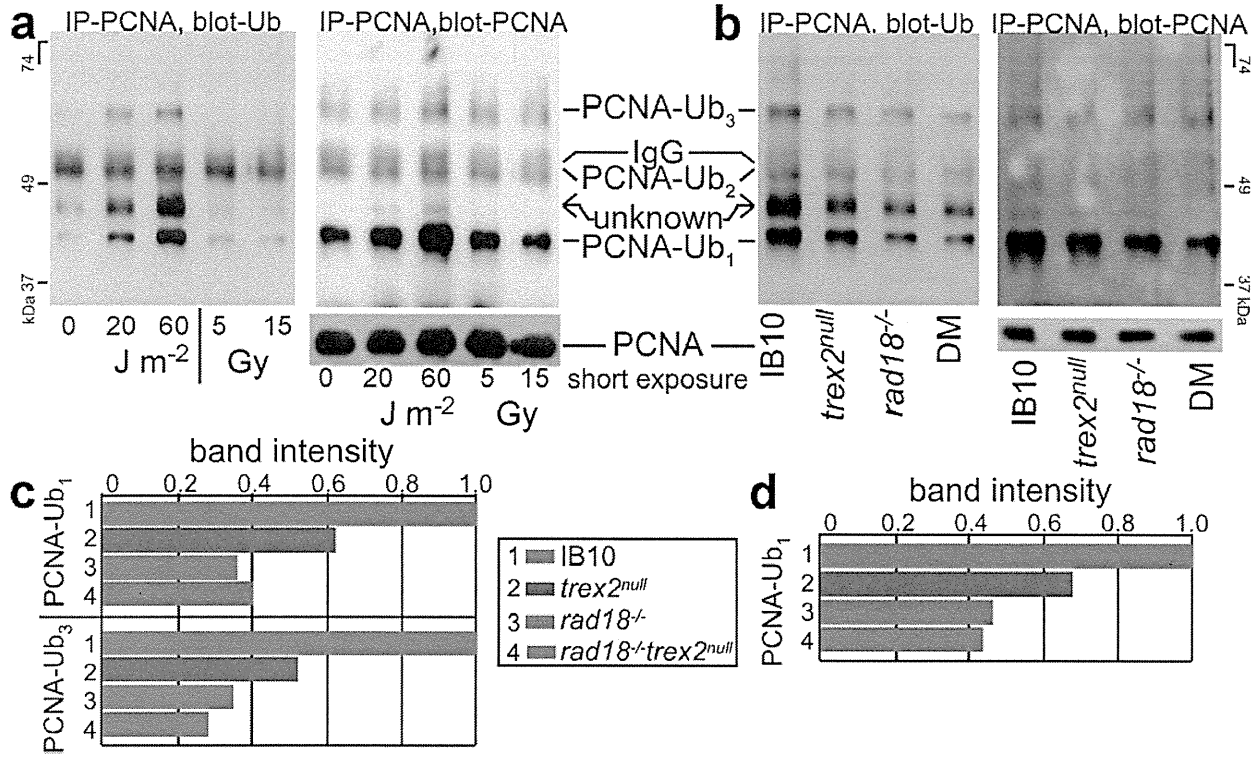

Extended Data Figure 6 | RAD18 and TREX2 ubiquitinate PCNA. **a**, Exposure of AB2.2 cells to ultraviolet light, but not γ-radiation, induced PCNA ubiquitination. Immunoprecipitate endogenous PCNA and immunoblot with anti-ubiquitin (Ub, left), then strip and immunoblot with anti-PCNA (right). PCNA–Ub_1 and PCNA–Ub_3 are visible; yet, IgG obscures PCNA–Ub_2. In addition, the Ub blot, but not the PCNA blot, reveals a previously unidentified band between PCNA–Ub_1 and PCNA–Ub_2. Ultraviolet light, but not γ-radiation, increased levels of PCNA–Ub_1 and PCNA–Ub_3 as previously shown in human cells[21] (the same was true for the unknown protein). Survival fraction: 20 J m^{-2}, 0.6%; 60 J m^{-2}, 0.06%; 5 Gy, 8%; 15 Gy; 0.001%. **b**, Analysis of *trex2*^{null} and *rad18*$^{-/-}$ cells and double-mutant cells. In response to 60 J m^{-2} ultraviolet light, *trex2*^{null} and *rad18*$^{-/-}$ cells had reduced levels of PCNA–Ub_1 and PCNA–Ub_3 and unknown protein as compared to IB10 cells. *rad18*$^{-/-}$ cells exhibited a marginally greater reduction than *trex2*^{null} cells, indicating that RAD18 has a greater role in PCNA ubiquitination. The double-mutant cells failed to show a further reduction, indicating that TREX2 and RAD18 are epistatic. Some ubiquitinated PCNA was present in mutant cells, indicating that other proteins ubiquitinate PCNA; similar observations were made for cells deleted for HLTF and SHPRH[40]. For example, $CRL4^{Cdt2}$, independent of RAD18, monoubiquitinates PCNA with and without ultraviolet-light-induced damage[47]. **c**, Bar graph illustrating the reduction of PCNA–Ub_1 and PCNA–Ub_3 in *trex2*^{null}, *rad18*$^{-/-}$, and double-mutant cells as shown in **b**, left (immunoprecipitation-PCNA, blot-Ub), after band intensities were quantified with ImageJ and normalized for loading with short exposure PCNA. Statistics (*t*-test) for PCNA–Ub_1 and PCNA–Ub_3 using three experiments (lanes): 1 vs 2 (0.0016, 0.0058), 1 vs 3 (0.0036, 0.0026), 1 vs 4 (0.0064, 0.0001), 2 vs 3 (0.0214, 0.0774), 2 vs 4 (0.0310, 0.0486), 3 vs 4 (0.3169, 0.1209). **d**, Bar graph illustrating the reduction of PCNA–Ub_1 in *trex2*^{null}, *rad18*$^{-/-}$, and double-mutant cells as shown in **b**, right (immunoprecipitation-PCNA, blot-PCNA), after band intensities were quantified with ImageJ and normalized for loading with short exposure PCNA. The stripping and re-probing leaves quantification unreliable for PCNA–Ub_3 and further work is required to clarify the extent to which Ub modification is influenced in these backgrounds. Statistics (*t*-test) for PCNA–Ub_1 using three experiments (lanes): 1 vs 2 (0.0021), 1 vs 3 (0.0061), 1 vs 4 (0.0460), 2 vs 3 (0.0212), 2 vs 4 (0.0163), 3 vs 4 (0.0604).

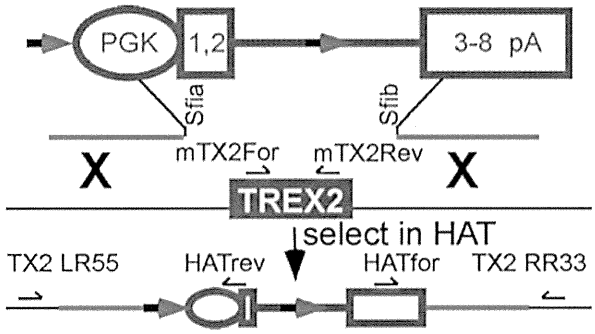

Extended Data Figure 7 | Deleting *Trex2* in IB10 control and *rad18*$^{-/-}$ cells. A floxed *MiniHPRT*[36] was used to replace the entire *Trex2* coding sequences (located on a single exon)[25]. Targeted clones were detected using PCR with TX2 LR55 and HATrev primers for the left arm and HATfor and TX2 RR33 primers for the right arm. Removal of the *Trex2* coding sequence was verified by PCR using mTX2For and mTX2Rev primers.

Extended Data Table 1 | IRR summary

clone	#MPS	DP	EPT	SD
1	32	3	0	0
2	32	0	0	0
3	30	3	0	0
4	33	0	0	0
5	25	1	0	0
6	31	1	0	0
7	30	0	0	0
8	23	1	0	0
9	27	2	0	0
10	24	1	0	0
11	27	0	0	0
12	31	0	2	0
13	47	0	1	0
14	53	0	2	0
15	65	2	1	0
16	46	0	1	0
17	48	1	1	0
18	49	1	0	0
19	54	0	1	1

Dipericentric (DP), extra pericentromere and telomere (EPT), metaphase spread (MPS), segmental duplication (SD).

Extended Data Table 2 | MRR summary

clone	#MPS	DP	EPT	SD
1	27	1	0	0
2	22	3	0	0
3	22	0	1	0
4	35	1	2	0
5	31	1	3	0
6	31	1	1	0
7	29	0	0	0
8	26	0	2	0
9	28	3	0	0
10	22	0	2	1
11	26	2	1	0
12	22	2	2	1
13	47	0	24	0
14	34	0	1	0
15	35	1	11	0
16	36	1	1	0
17	44	2	0	0
18	38	0	28	0
19	36	1	3	0

Dipericentric (DP), extra pericentromere and telomere (EPT), metaphase spread (MPS), segmental duplication (SD).

Extended Data Table 3 | Spectral karyotyping summary

MRR clone	nuclei	Simple EPT	Complex EPT	other
13	1	-	-	-
	2	Dup(1;1)	T(14;13)	-
	3	Dup(7;7)	T(3;13)	chromatid fusion (8;19)
	4	Dup(1;1)	T(14;13)	chromatid break (16)
	5	-	-	-
	6	-	T(14;13)	Del(1)
	7	chr1-chr4-chr17	T(14;13)	-
	8	Dup(1;1) Dup(7;7)	T(14;13) T(2;?)	Del(3)
	9	Dup(1;1)	-	-
15	1	Dup(1;1)	-	T(11;14) T(14;11)
	2	Dup(1;1)(1;)	-	T(11;14) T(14;13) Del(13)
	3	Dup(1;1)	T(?;13)	T(11;14) T(14;11)
	4	Dup(1;1)	-	T(11;3)
	5	Dup(1;1)	-	Ins(3;11) T(11;3) Del(3)
	6	Dup(1;1)	-	T(11;14) T(14;11)
	7	Dup(1;1)	-	T(11;14) T(14;11)
18	1	Dup(1;1) Dup(7;7)	T(14;11)	-
	2	-	T(14;11)	-
	3	Dup(1;1) Dup(12;12)	T(14;11)	-
	4	Dup(1;1)	T(14;11)	-
	5	-	T(14;11)	-
	6	Dup(1;1) Dup(7;7)	T(14;11)	-
	7	Dup(1;1) Dup(7;7)	T(14;11)	chromatid fusion (17;14)
	8	Dup(1;1) Dup(12;12)	T(14;11)	-

Simple extra pericentromere and telomere (EPT) involves one chromosome. Complex EPT involves more than one chromosome. Other has only one pericentromere.

Published online 23 January 2013

Nucleic Acids Research, 2013, Vol. 41, No. 5 3079–3093
doi:10.1093/nar/gkt016

A non-catalytic role of DNA polymerase η in recruiting Rad18 and promoting PCNA monoubiquitination at stalled replication forks

Michael Durando[1,*], Satoshi Tateishi[2] and Cyrus Vaziri[1,*]

[1]Department of Pathology and Laboratory Medicine, University of North Carolina at Chapel Hill, Chapel Hill, NC 27599, USA and [2]Division of Cell Maintenance, Institute of Molecular Embryology and Genetics (IMEG), Kumamoto University, Honjo 2-2-1, Kumamoto 860-0811, Japan

Received August 28, 2012; Revised December 13, 2012; Accepted December 24, 2012

ABSTRACT

Trans-lesion DNA synthesis (TLS) is a DNA damage-tolerance mechanism that uses low-fidelity DNA polymerases to replicate damaged DNA. The inherited cancer-propensity syndrome xeroderma pigmentosum variant (XPV) results from error-prone TLS of UV-damaged DNA. TLS is initiated when the Rad6/Rad18 complex monoubiquitinates proliferating cell nuclear antigen (PCNA), but the basis for recruitment of Rad18 to PCNA is not completely understood. Here, we show that Rad18 is targeted to PCNA by DNA polymerase eta (Polη), the *XPV* gene product that is mutated in *XPV* patients. The C-terminal domain of Polη binds to both Rad18 and PCNA and promotes PCNA monoubiquitination, a function unique to Polη among Y-family TLS polymerases and dissociable from its catalytic activity. Importantly, XPV cells expressing full-length catalytically-inactive Polη exhibit increased recruitment of other error-prone TLS polymerases (Polκ and Polι) after UV irradiation. These results define a novel non-catalytic role for Polη in promoting PCNA monoubiquitination and provide a new potential mechanism for mutagenesis and genome instability in XPV individuals.

INTRODUCTION

Living organisms are constantly exposed to ubiquitous genotoxins from endogenous and external sources (1). However, cells have evolved numerous DNA damage response (DDR) pathways that protect genomic DNA and prevent genetic instability (2). Trans-lesion synthesis (TLS) is a DDR mechanism involving specialized DNA polymerases that can replicate damaged DNA templates (3).

TLS relies on inherently error-prone DNA polymerases of the Y family to replicate damaged DNA (4). TLS by Y-family polymerases (Polη, Polι, Polκ and Rev1) (5) maintains replication in cells harbouring damaged DNA, albeit at the cost of reduced fidelity. Each TLS polymerase performs relatively error-free replication past a preferred cognate lesion; in the absence of the appropriate TLS polymerase for its preferred lesion, mutagenic replication by error-prone polymerases predisposes to genetic instability (2).

Polη is unique among Y-family polymerases in its ability to perform accurate replication past UV-damaged DNA (6,7). Lack of Polη in the inherited cancer-propensity syndrome xeroderma pigmentosum variant (XPV) (8) results in error-prone replication by other Y-family polymerases in sunlight-exposed cells (9,10). Thus, UV-induced mutagenesis due to Polη deficiency compromises genetic integrity to manifest as exquisite sunlight sensitivity and early skin cancer propensity.

A prerequisite for error-prone replication in TLS is the Rad6/Rad18-mediated monoubiquitination of proliferating cell nuclear antigen (PCNA) at the highly conserved lysine K164 (11,12). Y-family polymerases contain ubiquitin-binding (UBZ) domains that confer affinity to monoubiquitinated PCNA (13,14). Failure to monoubiquitinate PCNA at K164 phenocopies XPV by compromising TLS and sensitizing cells to UV light and other ubiquitous genotoxins (15–18). Several other DDR pathways also depend on PCNA monoubiquitination, including SHPRH/HTLF-mediated template switching (19), ZRANB3-dependent replication fork restart (20), SNM1A-dependent intrastrand cross-link repair (21) and the Fanconi Anaemia pathway activation (22).

Despite its pivotal role in the DDR, the molecular mechanisms regulating Rad18-mediated PCNA monoubiquitination are incompletely understood. The Rad18–Rad6 complex is thought to be recruited to the vicinity of damaged DNA via direct interactions with RPA-coated

*To whom correspondence should be addressed. Tel: +1 617 818 3441; Fax: +1 919 966 5046; Email: mdurando@med.unc.edu
Correspondence may also be addressed to Cyrus Vaziri. Tel: +1 919 843 9630; Fax: +1 919 966 5046; Email: cyrus_vaziri@med.unc.edu
Present address:
Michael Durando, Department of Pathology and Laboratory Medicine, University of North Carolina at Chapel Hill, Chapel Hill, NC 27599, USA.

ssDNA (23,24). However, Rad18 lacks PCNA-binding motifs, and it is unclear how Rad18 is targeted specifically to PCNA at stalled forks (or other sites of post-replication repair). A recent report by Zou and colleagues (25) identified Spartan as a binding partner of both Rad18 and PCNA and proposed that Spartan acts as a scaffold for recruiting Rad18 to PCNA. Consistent with a role for Spartan in targeting Rad18 to PCNA, those workers found DNA damage-induced PCNA monoubiquitination was modestly attenuated in Spartan-depleted cells. However, several other more recent publications have reported alternative roles for Spartan in DNA damage signalling (26–29), and it is unclear whether Spartan or alternative putative mediators exist to facilitate recruitment of Rad18 to PCNA.

In mammalian cells, Rad18 exists in complex with Polη (30,31), and association of Rad18 with Polη is necessary for normal DNA damage tolerance (30–32). Assembly of the Rad18–Polη complex is stringently controlled by Cdc7 and Chk1 kinases, which serve to integrate TLS with S-phase progression and the S-phase checkpoint, respectively (30,32). Here we report that the Polη–Rad18 interaction plays a key role in targeting Rad18 to PCNA and facilitating efficient PCNA monoubiquitination. Interestingly, the novel role of Polη in stimulation of PCNA monoubiquitination is fully dissociable from its activity as a DNA polymerase. We show that the Polη–Rad18 interaction provides the basis for coupling PCNA monoubiquitination with DNA damage-inducible checkpoint pathways mediated by p53 and Chk1. Our results also provide a potential explanation for numerous reports that Polη confers tolerance of non-cognate lesions (33,34) and that catalytically inactive Polη can partially rescue the DNA damage-sensitivity phenotypes of XPV cells (35,36). Moreover, because some XPV cells express a catalytically inactive Polη that retains the ability to promote PCNA monoubiquitination, our results also indicate a new molecular mechanism for the mutagenesis and cancer propensity of XPV patients.

MATERIALS AND METHODS

Cell culture and transfection

H1299, HDF, XP115LO [GM02359(37,38)] and HCT-116 WT and Rad18$^{-/-}$ cells (39) were cultured in Dulbecco's modified Eagle medium (DMEM) supplemented with 10% fetal bovine serum (FBS) and penicillin–streptomycin. SiRNA and pcDNA, pACCMV and pCAGGS plasmid transfections were done using Lipofectamine 2000 (Invitrogen) as previously described (30).

Materials, siRNA, plasmid and adenovirus construction

siRNA oligonucleotide sequences were as follows: non-targeting Control, 5′–UAGCGACUAAACACAUC AAUU–3′; Polη, 5′–GCAGAAAGGCAGAAAGUUA–3′; Polη-3′ UTR, 5′–CCAUUUAGGUGCUGAGUUA–3′; Polη-5′ UTR, 5′–GAAUAAAUCUCGCUCGAAA–3′; Chk1, 5′–GCGUGCCGUAGACUGUCCA–3′; USP1, 5′–TCGGCAATACTTGCTATCTTA–3′; Polκ, 5′–GUAAAGAGGUUAAGGAAA–3′; Rad18 3′ UTR, 5′–UUAUAAAUGCCCAAGGAAAUU–3′; Spartan 5′–ACCGGACUUGCAGGCACUGUUUGUU–3′. CFP was cloned onto the C-terminus of Rad18 in pACCMV using BamH1 and Xba1 restriction sites. Rad18 and CFP were separated by a linker of the sequence 5′–ACCTCTT CCGGTTCCAGTCCCTGTTCCGGGTCCTGCTCCT ATGCGTATGGCTCC–5′. Rad18-Δ(402–445) and Rad18-C28F were generated as described previously (31) and cloned into pACCMV using EcoRI and BamHI restriction sites. Polη-ΔPCNA-interacting peptide (PIP) was cloned into pACCMV using EcoRI and BamHI restriction sites and a C-terminal primer containing phenylalanine to alanine mutations at AA 705 and 707. Catalytically inactive Polη was generated by mutating codons D13, E22, D115 and E116 to alanine in the N-terminal catalytic active site to disrupt coordination of Mg^{2+} ions between dNTP, primer and active site moieties and block nucleotide incorporation(40); this construct was then cloned into pACCMV using EcoRI and BamHI restriction sites. N-terminal Polη truncations were generated with 5′ and 3′ primers containing EcoRI and BamHI restriction sites, respectively, and cloned into pACCMV. The Rad18–Polη fusion was constructed by PCR amplification of Polη with primers containing 3′ BamHI and 5′ XbaI restriction sites, followed by ligation into pACCMV-Rad18. Polη-ΔPLTH and Polκ+PLTH were generated with C-terminal primers omitting or adding, respectively, codons for the PLTH domain, followed by a BamHI restriction site for ligation into pACCMV. pDEST-SFB-Spartan was obtained from Lee Zou (MGH Cancer Center). Adenovirus constructions were performed by recombination of pACCMV constructs with pJM17 as described previously (41).

Adenoviral expression and titration

Adenoviral infection was performed as described previously by adding to cultured cells CsCl-purified adenovirus (41). Infections in H1299 cells were typically done at 0.1–1.0 × 10^9 pfu/ml and in XPV/HDF cells at 0.1–5.0 × 10^9 pfu/ml. Titration to expression levels approximately equal to endogenous was done by serial infections followed by immunoblotting of extracts with antibodies against the endogenous protein.

Fluorescence microscopy

H1299 or XPV cells were grown to ~60% confluency on glass-bottom plates (Mat-tek) and then infected with adenovirus (CFP-Rad18-WT, YFP-Polη, GFP-Polκ and respective mutants) to achieve expression approximately equal to endogenous as determined by Western blot. For co-expression and knockdown experiments, co-infection or transfection was performed 6 h before adenoviral infection. Twenty hours after infection, cells were exposed to genotoxins and then prepared for live or fixed-cell imaging on a Zeiss 710 confocal microscope. For high-magnification representative images, Z-stacks at 0.5-μm intervals were collected throughout the entire cell volume using a 63× oil-immersion objective and 2.3× optical zoom. 3D projections of Z-stacks were performed